JOURNAL OF MATERIALS SCIENCE 33 (1998) 1217–1225

High-temperature strength and thermal stability of a unidirectionally solidified Al_2O_3/YAG eutectic composite

Y. WAKU, N. NAKAGAWA, T. WAKAMOTO, H. OHTSUBO, K. SHIMIZU, Y. KOHTOKU
Ube Research Laboratory, Corporate Research & Development, UBE Industries Ltd., Ube City, Yamaguchi, 755, Japan
E-mail: 25222u@ube-ind.co.jp

A unidirectional solidification method was investigated to manufacture Al_2O_3/YAG eutectic composites with high-temperature resistance that would make them usable at very high temperatures. We were successful in manufacturing a single-crystal Al_2O_3/single-crystal YAG eutectic composite with a dimension of 40 mm in diameter and 70 mm in length containing no colonies or pores. This composite also displayed excellent high-temperature strength characteristics. The flexural strength was in the range 350 $\sim$ 400 MPa from room temperature up to 2073 K (just below its melting point of about 2100 K) with no apparent temperature dependence. During tensile tests above 1923 K, the eutectic composite showed evidence of plastic deformation occurring by dislocation motion, and a yield phenomenon similar to many metals was observed. In addition, the microstructure of the composite was extremely stable: after 1000 h of heat treatment at 1973 K in an air atmosphere there was no growth. The above superior high-temperature characteristics are caused by such factors as the eutectic composite having a single-crystal Al_2O_3/single-crystal YAG structure, the formation of a compatible interface with no amorphous phase and thermal stability, and the combined effect of a YAG phase with superior high-temperature characteristics.

1. Introduction

To improve thermal efficiency in jet aircraft engines and high-efficiency power-generation gas turbines, the engines or turbines should run at higher temperatures. To achieve this, there is strong need to develop a material that remains stable at very high temperatures. A wide range of options ranging from monolithic ceramics (e.g. SiC or Si_3N_4) to ceramic–matrix composites (CMC) is in progress on a global scale. However, because SiC and Si_3N_4 show extreme oxidation in ambient atmosphere at high temperatures above 1773 K, they are not stable for long term use in such environments. Internationally, the material usable at the highest temperature is currently SiC/SiC composites [1] manufactured by SEP (Société Européene de Propulsion) using CVI (chemical vapour infiltration) methods. While this material has high fracture toughness and is stable at high temperatures, further improvement is required so it can be used at temperatures above 1673 K in an air atmosphere.

Because oxide ceramics in general are very susceptible to plastic deformation at high temperatures, they have not been considered as structural materials at high-temperature applications. However, these oxide ceramics are better than other ceramics in their oxidation resistance at high temperatures, [2], and if their mechanical properties at high temperatures can be improved, they are expected to find a wide range of expanding uses as structural materials at elevated temperatures.

Sintering of compacted powders constitutes the main manufacturing method of ceramics today. Because of improvements in powder characteristics, such as finer and higher purity powders, and because manufacturing takes place under highly controlled sintering conditions, it is now possible to manufacture high-strength ZrO_2 ceramics with a strength of around 3.0 GPa at room temperature [3]. Moreover, the powder sintering process enables the manufacture of composites with nanodistribution of different types of ceramic particles, and improvements can be obtained in many physical properties: e.g. strength, toughness, and heat characteristics [4–7]. However, in particular, the mechanical properties of ceramic composites at high temperatures are greatly affected by the structure of the interface of the composing materials, and by the crystallographic characteristics of both the reinforcing phase and matrix. Therefore, instead of using conventional sintering processes, it is important to develop new ceramic manufacturing methods that allow precise control of these parameters.

D. Viechnicki *et al.* [8] conducted microstructural studies on a $Al_2O_3/Y_3Al_5O_{12}$ (YAG) system using the Bridgman method, and showed that microstructure of

the eutectic composite could be controlled by unidirectional solidification. In addition, it has recently been reported that a unidirectionally solidified Al_2O_3/YAG eutectic composite has superior flexural strength, thermal stability and creep resistance at high temperature [9–11], and is a candidate for high-temperature structural materials. However, as it consists of many colonies, being composed of a eutectic microstructure of Al_2O_3 and YAG, a fairly strong influence of colony boundaries is in prospect. On the other hand, Waku *et al.* [12–14] have recently fabricated a eutectic composite consisting of a single crystal Al_2O_3 and a single crystal YAG with neither colonies nor grain boundaries, using a unidirectional solidification method. The composite fabricated is thermally stable and has the following properties: (1) the flexural strength at room temperature can be maintained up to 1973 K, (2) the compressive creep strength at 1873 K and a strain rate of $10^{-4}\,s^{-1}$ is about 10 times higher than that of sintered composites with the same composition, (3) it shows neither weight gain nor grain growth, even upon heating at 1973 K in an air atmosphere for 50 h.

Accordingly, in order to confirm the superior high temperature characteristics of this composite by a still larger sample, the primary objective of this research is to manufacture a specimen of 40 mm in diameter and 70 mm in length using Bridgman-type equipment, while the secondary objective is to investigate characteristics such as the structural phase and interface structure of the composite obtained, the temperature dependence of its strength, and the thermal stability of its microstructure.

2. Experimental procedure

2.1. Manufacturing of raw powders

Using commercially available Al_2O_3 powder (AKP-30, produced by Sumutomo Chemical Co., Ltd) and Y_2O_3 powder (Y_2O_3-RU, submicron-type, produced by Shin-Etsu Chemical Co., Ltd), wet ball-milling of a $Al_2O_3/Y_2O_3 = 82/18$ mol ratio was undertaken to obtain a uniform composite powder slurry. After removing the ethanol and drying the slurry using a rotary evaporator, high-frequency induction heating to a Mo crucible (50 mm in diameter by 200 mm in length by 5 mm thickness) was applied to perform preliminary melting and obtain an ingot.

2.2. Unidirectional solidification

All experiments were performed using the Bridgman-type equipment at the Japan Ultra-high Temperature Materials Research Center. Fig. 1 shows the unidirectional solidification equipment used. The ingot obtained by preliminary melting was inserted into Mo crucible (50 mm in outside diameter by 200 mm in length by 5 mm in thickness) placed in a vacuum chamber, and a graphite susceptor was heated by high-frequency induction heating. This heated the Mo crucible and facilitated the melting. After sustaining the melt of 2223 K (about 120 K above melting point of approximately 2100 K) for 30 min, the Mo crucible was lowered at $5\,mm\,h^{-1}$, completing the unidirectional solidification experiment.

2.3. Sintering

Mixed powders obtained using ball milling were hot-pressed in a carbon die to fabricate composite of $50 \times 70 \times 5$ mm at 1973 K under a 50 MPa pressure for an hour in a vacuum (10^{-2} mmHg).

2.4. Evaluation Process

The specimens used for the three-point flexural test and the tensile test were selected so that their axial direction was parallel to the direction of the unidirectional solidification. The dimensions of the flexural test specimen were $3 \times 4 \times 36$ mm with a 30-mm span, while the dimensions and shape of the tensile test specimen are shown in Fig. 2. The three-point flexural

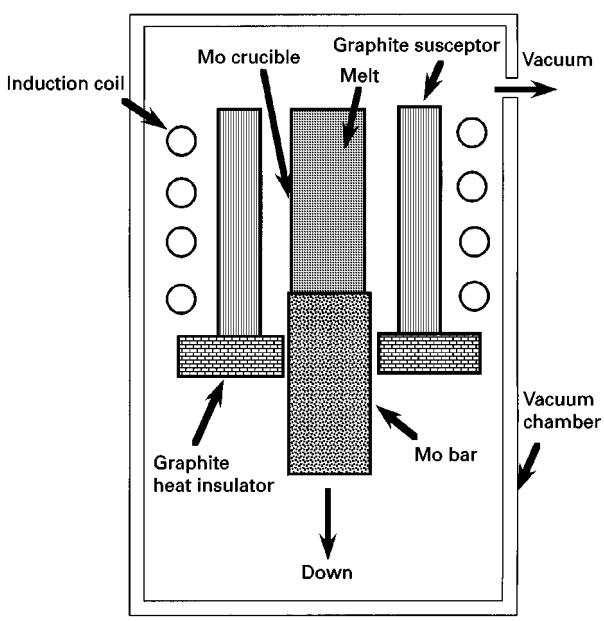

Figure 1 Bridgman-type equipment used in unidirectional solidification experiments.

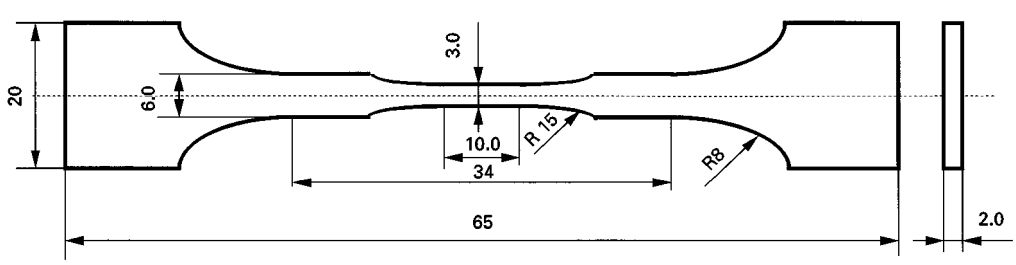

Figure 2 Shape and dimensions of tensile test specimens.

strength was measured from room temperature to 2073 K in an argon atmosphere at a cross-head speed of 0.5 mm min^{-1}. The tensile tests were also conducted at a strain rate of 10^{-4} s^{-1} in an argon atmosphere from room temperature to 2023 K. The tests were carried out using the high-temperature uniaxial tension-compression and flexural test system (modified creep and fatigue machine, type 8562 produced by Instron) at the Japan Ultra-high Temperature Materials Research Center. The thermal stability of the microstructure of the composite fabricated was evaluated from microstructural changes after heat treatment in an air atmosphere at 1973 K for up to 1000 h using electric furnace with kanthal super 1900 heater.

Microstructural characterization was performed using the RAD-RB-type X-ray diffraction equipment produced by Rigaku Denki. High-resolution transmission microscopic (HRTEM) observation of the interface of the Al_2O_3 and the YAG phases was carried out using a JEM-2010 produced by Japan Electron, while the electron probe microanalysis (EPMA) was conducted with a JMX-8621MX by Japan Electron.

3. Results and discussion

3.1. Microstructure of unidirectionally solidified eutectic composites

Fig. 3 shows the scanning electron microscope (SEM) image and the EPMA analysis results. Fig. 4a and b show X-ray diffraction patterns of the eutectic composite obtained from a cross-section perpendicular to and a cross-section declined by about 76° from the solidification direction of the composite, respectively. Fig. 4c shows the X-ray diffraction pattern of a crushed powder of the as-grown eutectic composite, which is the same sample as used for the X-ray diffraction shown of Fig. 4a and b. In case of the as-grown composite, strong diffraction from the YAG (7 4 3) plane was observed in Fig. 4a, whereas only strong diffraction from the Al_2O_3 (1 1 0) plane was observed in Fig. 4b. It can be deduced from the comparison between Fig. 4a, b and c that the as-grown composite consisted of a $\langle 7\,4\,3 \rangle$ single-crystal YAG and a $\langle 1\,1\,0 \rangle$ single-crystal Al_2O_3 (sapphire). From Fig. 3b, c and Fig. 4, it was clear that the white phase in Fig. 3a was the $\langle 7\,4\,3 \rangle$ single-crystal YAG and the black phase was the $\langle 1\,1\,0 \rangle$ single-crystal Al_2O_3.

Fig. 5 is a SEM photograph of the cross-section perpendicular to the solidification direction of the unidirectionally solidified eutectic composite. The eutectic composite is shaped very much like "hieroglyphics", consisting of single crystal Al_2O_3 with an irregular distribution at the microscopic level, and single crystal YAG. At the macroscopic level, the unidirectionally solidified eutectic composite has a uniform microstructure with no colonies or pores.

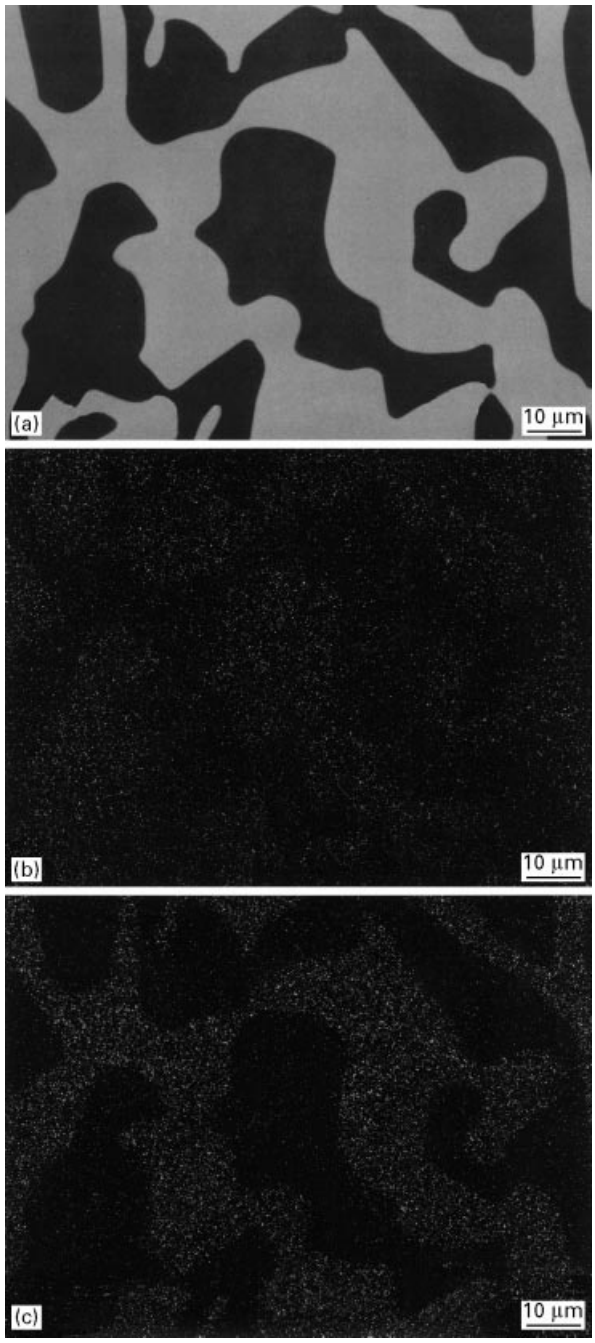

Figure 3 SEM image and EPMA analysis of the cross-section perpendicular to the solidification direction for the unidirectionally solidified eutectic composites. (a) SEM image, (b) EPMA analysis of Al element, and (c) EPMA analysis of Y element.

3.2. Microstructure of sintered composites

Fig. 6 is an X-ray diffraction pattern and Fig. 7 is a SEM photograph of microstructure of a sintered composite. From the X-ray diffraction results, it can be seen that the sintered composite is a polycrystalline material made up of the Al_2O_3 and YAG phases, and that the sintered composite has a completely different microstructure including grain boundaries between the Al_2O_3 phase, the YAG phase, and the Al_2O_3/YAG phase from the unidirectionally solidified eutectic composite without grain boundaries. This is a finer microstructure than the microstructure of the unidirectionally solidified eutectic composite.

3.3. Temperature dependence of the flexural strength

Fig. 8 shows the temperature dependence of the flexural strength of a unidirectionally solidified eutectic composite from room temperature to 2073 K in

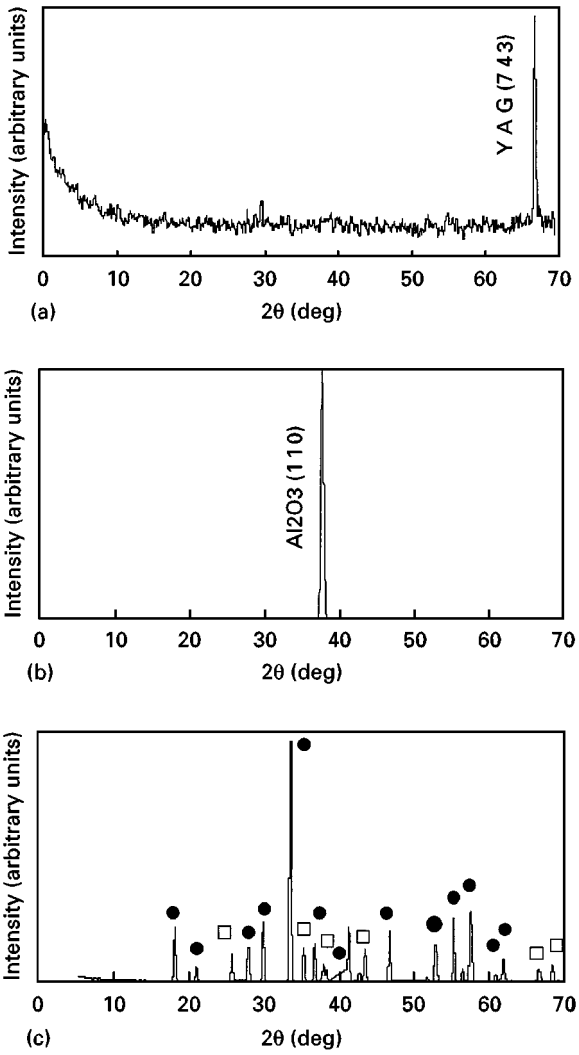

Figure 4 X-ray diffraction patterns of unidirectionally solidified eutectic composite at (a) plane perpendicular to the solidification direction, (b) at a plane 76° inclined to the solidification direction, and (c) powder fragmented from a unidirectionally solidified eutectic composite. (●) YAG; (□) Al_2O_3.

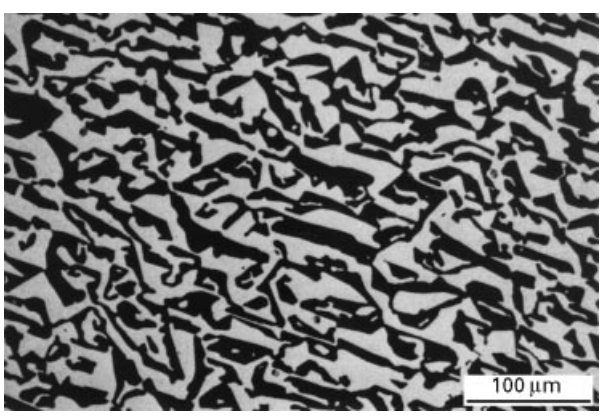

Figure 5 A typical SEM image of the microstructure of cross-section perpendicular to the solidification of a unidirectionally solidified eutectic composite.

comparison with that of a sintered composite of the same composition. The eutectic composite maintains its room temperature strength up to 2073 K (just below its melting point of about 2100 K), with a flexural strength in the range of 350 ~ 400 MPa. The sintered composite, on the other hand, has the same or higher flexural strength at room temperature, but its strength falls precipitously above 1073 K.

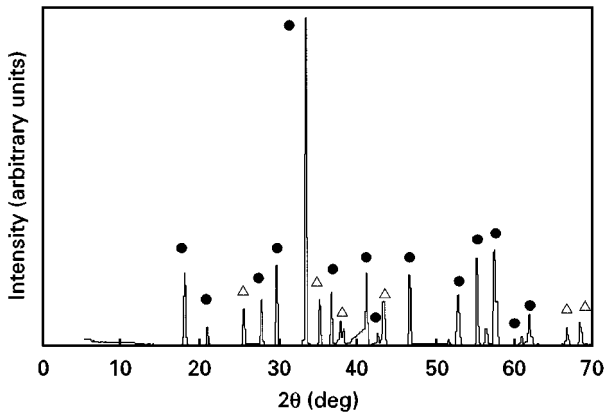

Figure 6 X-ray diffraction patterns of a sintered composite. (●) YAG; (△) Al_2O_3.

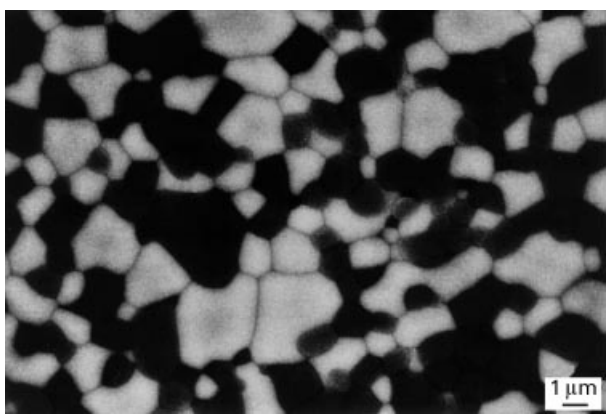

Figure 7 A typical SEM image of the microstructure of a sintered composite.

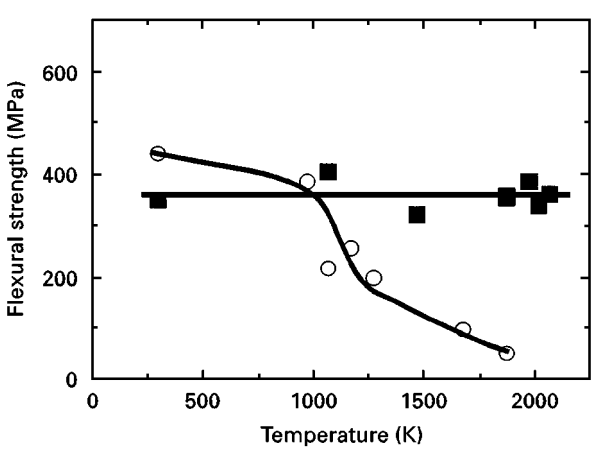

Figure 8 Temperature dependence of flexural strength of unidirectionally solidified eutectic composites (■) compared with sintered composites (○).

Fig. 9 is a SEM image of the fracture surface of a unidirectionally solidified eutectic composite and sintered composite. Sintered composites show intergranular fracture at room temperature and at 1673 K and evidence for grain growth is clear. On the other hand, the unidirectionally solidified eutectic composites show no grain growth up to the very

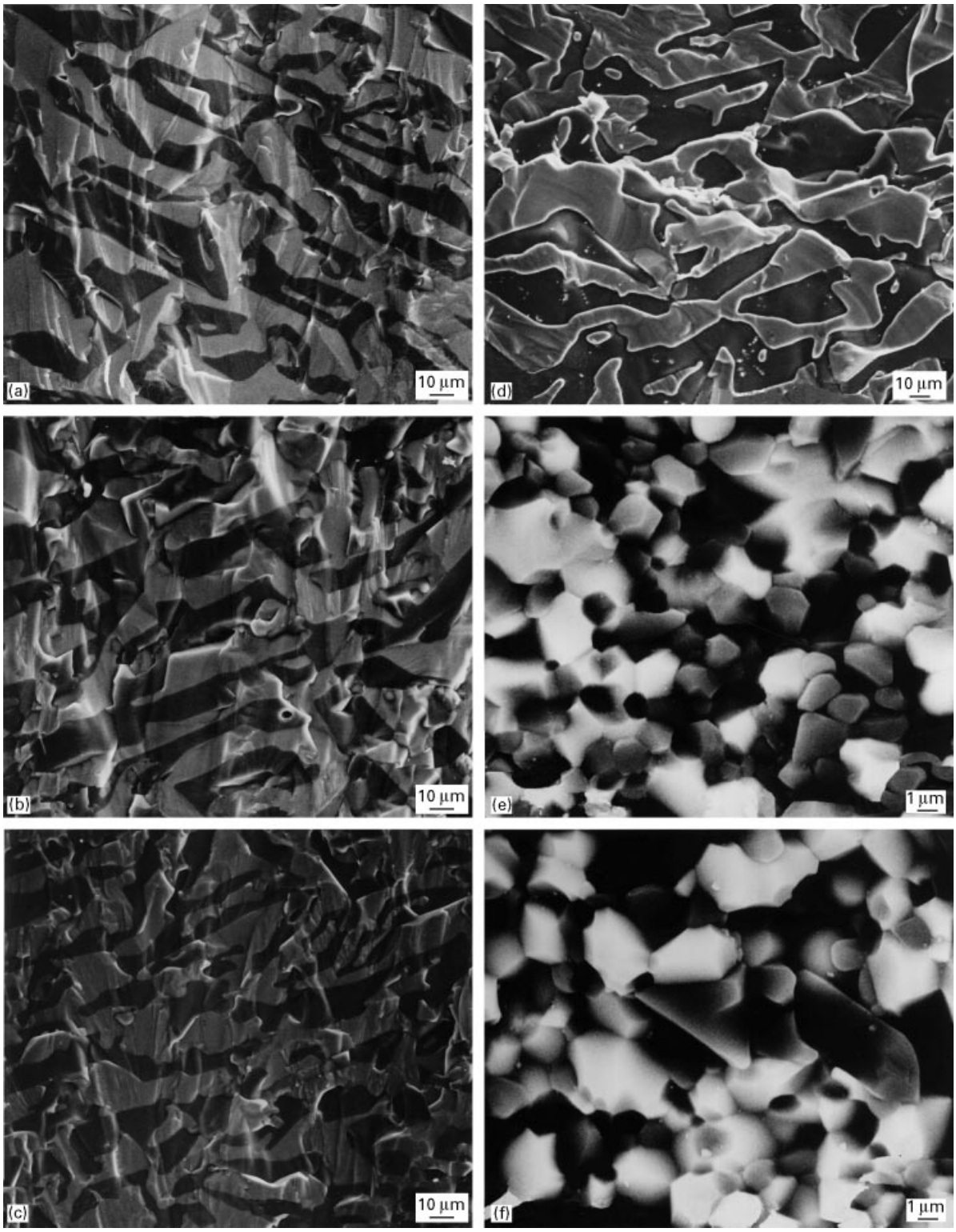

Figure 9 SEM photographs showing fracture surfaces in flexural tested specimens. For a unidirectionally solidified eutectic composite: (a) at room temperature, (b) at 1873 K, (c) at 1973 K, and (d) at 2073 K. For a sintered composite: (e) at room temperature and (f) at 1673 K.

high temperature of 1973 K, and the fracture is transgranular. Moreover, as shown in Fig. 9d, when the test temperature reaches 2073 K, fracture of the interface between Al_2O_3 and YAG phases and mixed fracture of intergranular and transgranular is observed.

Generally, if an interface or a grain boundary contain an amorphous phase, high-temperature strength is reduced [15, 16]. Fig. 10 shows HRTEM images of the grain boundaries between the Al_2O_3 and YAG phases of a sintered composite and the interface between the Al_2O_3 and YAG phases of a unidirectionally solidified eutectic composite. As we can see from Fig. 10a the sintered composite interface contains an amorphous phase. However, as is evident from Fig. 10b, the interface between the Al_2O_3 and YAG phases in the eutectic composite contains no amorphous phase.

From the above, it may be concluded that the superior high temperature strength was obtained by the following means: good crystal orientation of

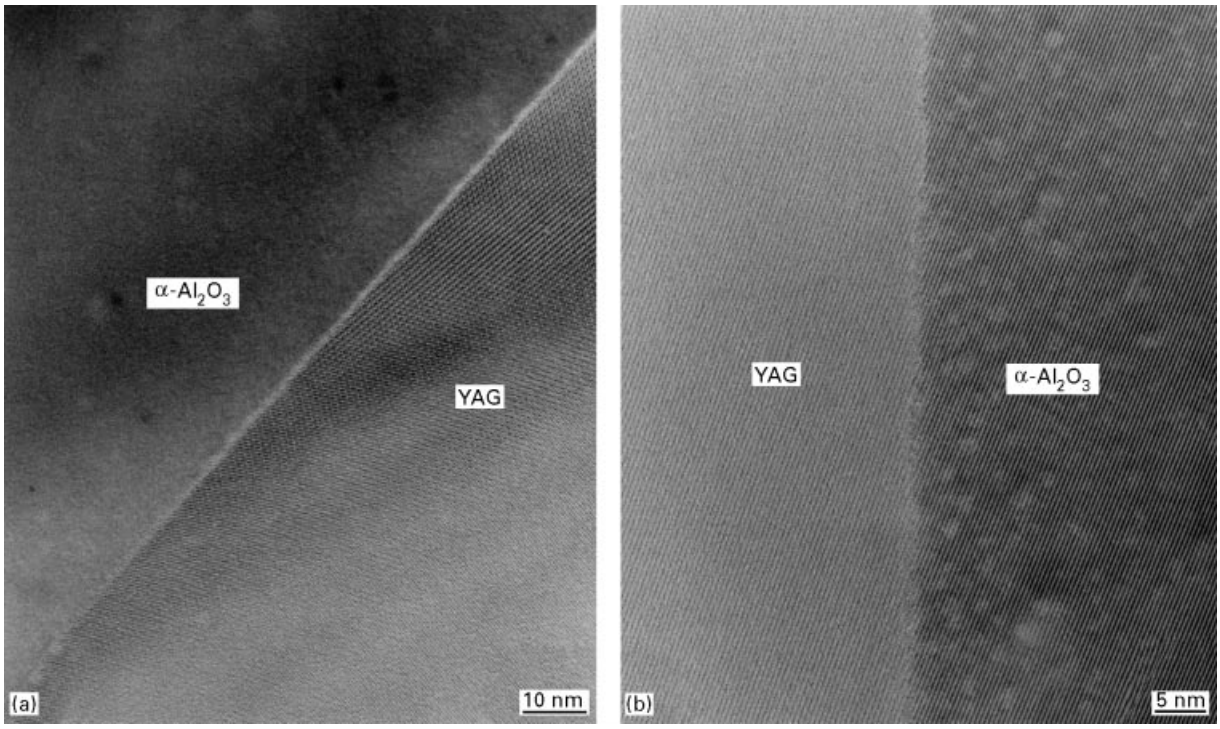

Figure 10 HRTEM images of (a) the grain boundary between the Al_2O_3 and YAG phases in a sintered composite and (b) the interface between Al_2O_3 and YAG phases of a unidirectionally solidified eutectic composite.

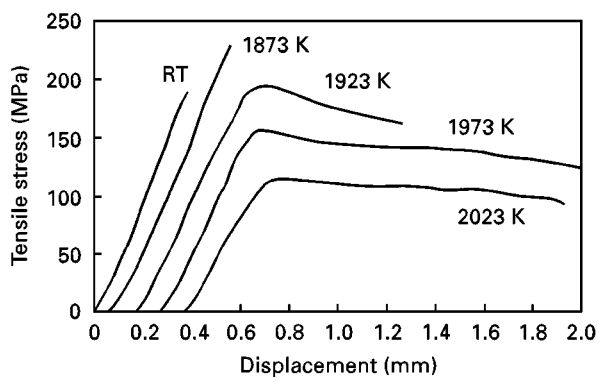

Figure 11 Tensile stress–displacement curves of a unidirectionally solidified eutectic composite from room temperature to 2023 K.

matrix, consisting of ⟨1 1 0⟩ single crystal Al_2O_3 and ⟨7 4 3⟩ single crystal YAG; no amorphous phases formed at interface between Al_2O_3 phases and YAG phases, which can easily cause plastic deformation; and the effect of the eutectic composite consisting of single crystal Al_2O_3 and YAG, which are stable at very high temperatures.

3.4. Tensile deformation

Fig. 11 shows the stress–displacement curve obtained from tensile tests of unidirectionally solidified eutectic composite from room temperature to 2023 K. Above 1923 K a yield phenomenon occurs and the composites fracture after around 10 ~ 20% plastic deformation. The yield stress is about 200 MPa at 1923 K. Fig. 12 shows a SEM image of the microstructure after plastic deformation caused by tensile testing at 1923 and 2023 K. As the photograph reveals, several cracks appeared in the microstructure at both the

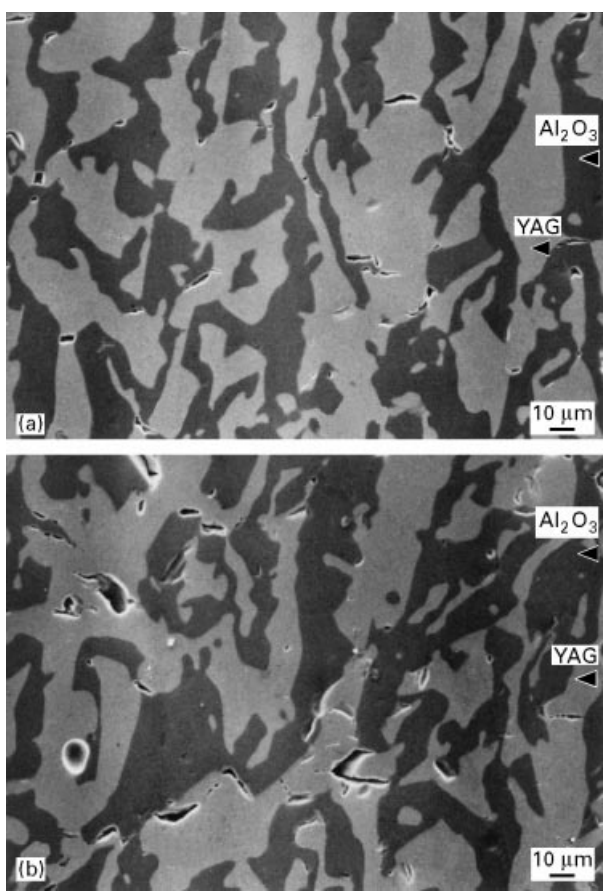

Figure 12 SEM images of the microstructure after tensile-caused plastic deformation of a unidirectionally solidified eutectic composite: (a) at 1923 K and (b) at 2023 K.

1923 and 2023 K temperature levels. Nearly all of the cracks were in the YAG phase, with almost none observed in the Al_2O_3 phase. Fig. 13 shows a SEM photograph of the fracture surface at tensile testing at

1973 K. This photograph shows a constricted area in which ductile fracture can be observed in the Al_2O_3 phase. In part of the photograph, dimple-shaped fracture surface can also be observed. Also, the type of fracture is mixed; intergranular and transgranular fracture are both present.

Fig. 14 shows TEM images of dislocation structures observed in the plastically deformed specimen in the tensile test at 1973 K for the unidirectionally solidified eutectic composites. Though the dislocation structures are to be observed in both single crystal Al_2O_3 and single crystal YAG, showing that the plastic deformation occurred by dislocation motion, dislocation densities and dislocation structures in both phases are largely different corresponding to microstructures in Fig. 12. Namely, many linear dislocations are observed in single crystal Al_2O_3 and meanwhile, low dislocation density is observed in single crystal YAG. The dislocation structures observed also indicate that the plastic deformation mechanism of the present eutectic composite is essentially different from that of micrograin superplasticity of ceramics [17] because of a grain-boundary sliding or a liquid phase present at grain boundary at high temperature.

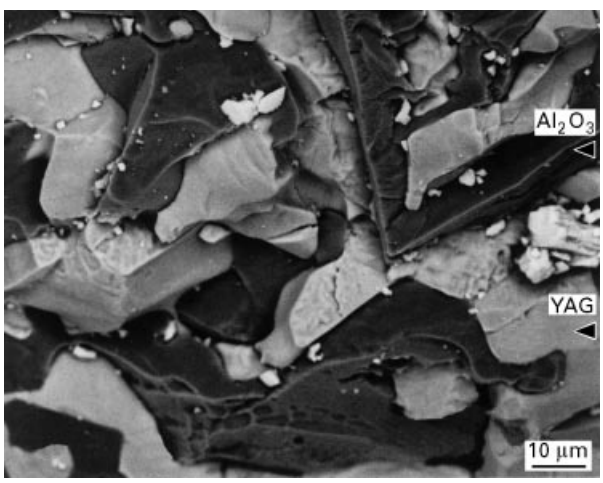

Figure 13 SEM image of a tensile fracture surface of a unidirectionally solidified eutectic composite tested at 1973 K.

3.5. Thermal stability of microstructure

Fig. 15 shows SEM images of the microstructure after 500, 750 and 1000 h of heat treatment at 1973 K in an air atmosphere. Even after 1000 h of heat treatment no grain growth of microstructure was observed. The unidirectionally solidified eutectic composite was shown to be very stable during lengthy exposure at high temperature of 1973 K in an air atmosphere. This stability resulted from the thermodynamic stability at that temperature of the constituent phases of the single-crystal Al_2O_3 and the single-crystal YAG, and the thermodynamic stability of the interface.

4. Conclusions

Using Bridgman-type equipment and the unidirectional solidification method, a Al_2O_3/YAG eutectic

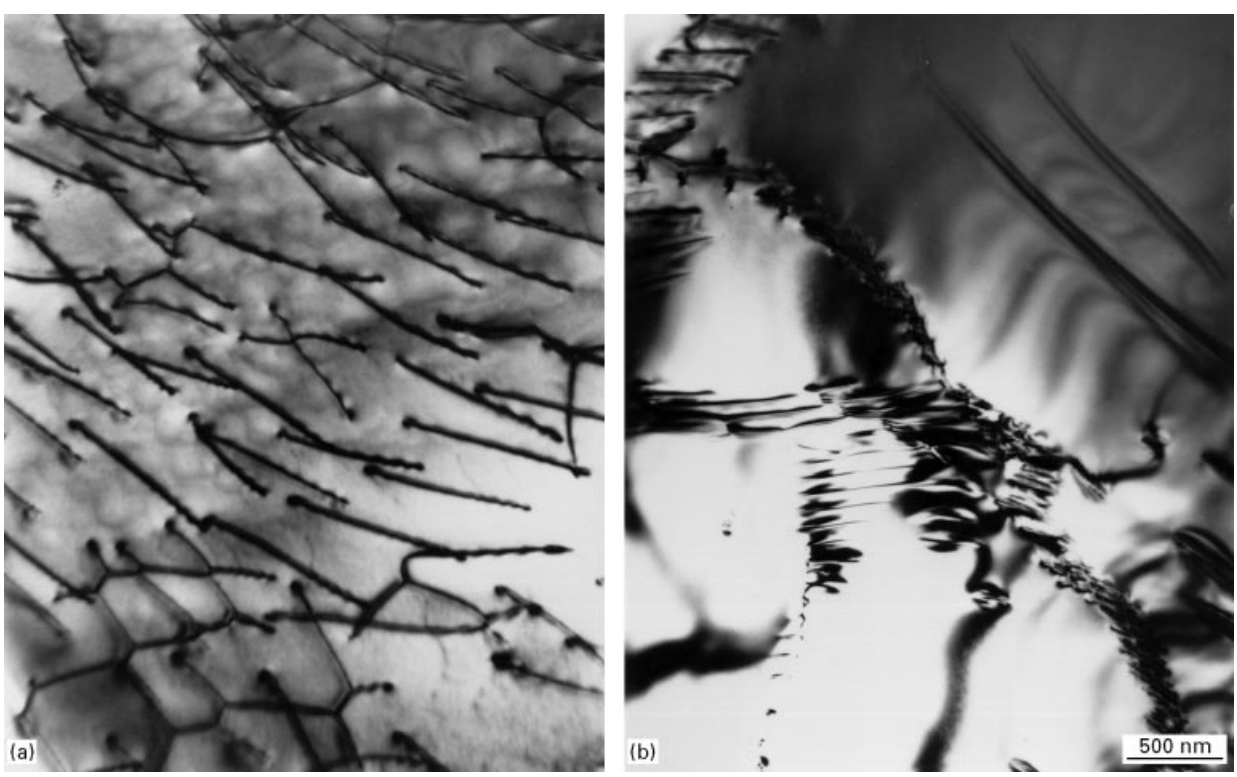

Figure 14 TEM images showing the dislocation structures of (a) Al_2O_3 phases and (b) YAG phases of the plastically deformed specimens after the tensile test at 1973 K of the unidirectionally solidified eutectic composites.

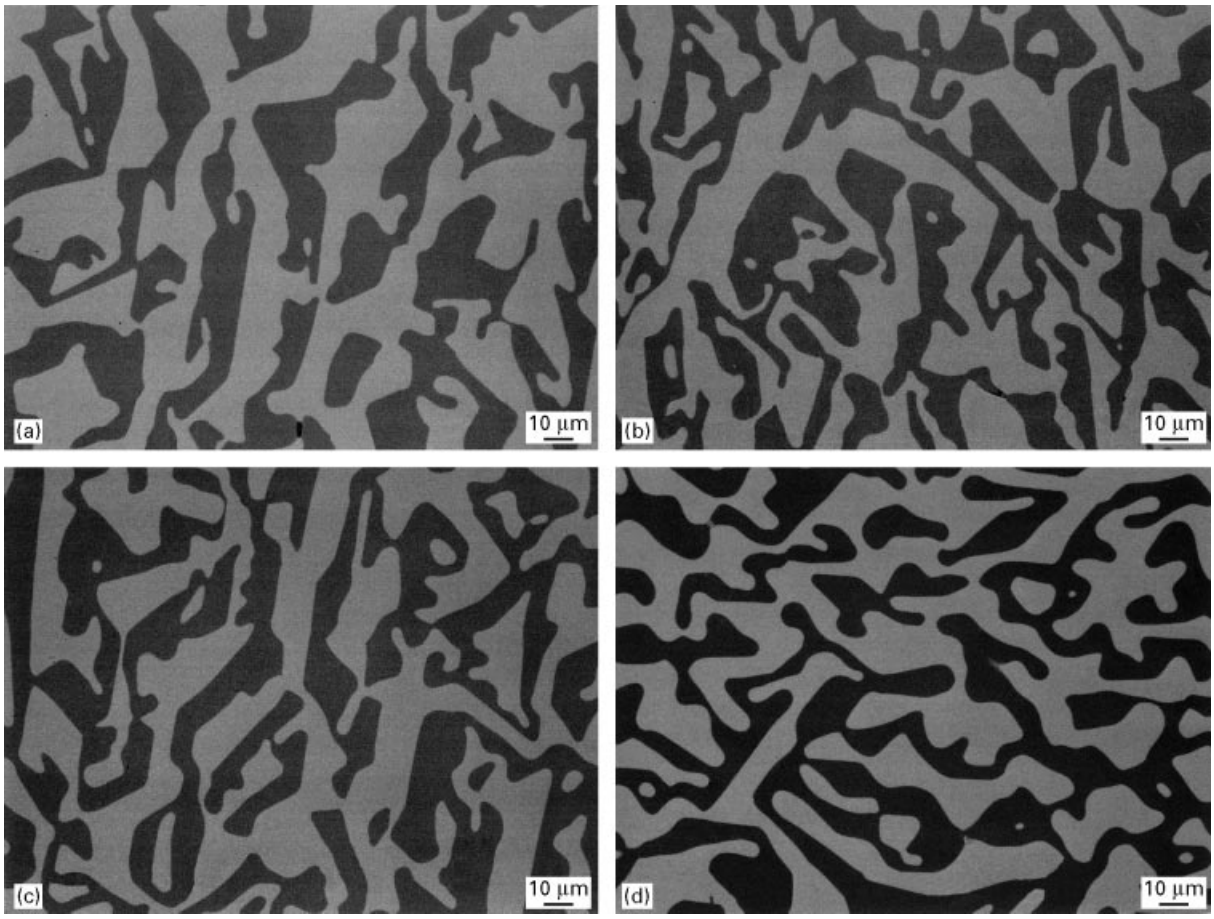

Figure 15 Thermal stability of the microstructures of a unidirectionally solidified eutectic composite at 1973 K in an air atmosphere. (a) as-received and after heat treatment (b) for 500 h, (c) 750 h, and (d) 1000 h.

composite with a dimension of 40 mm in diameter and 70 mm in height was fabricated.

The eutectic composite was consisted of a $\langle 1\,1\,0 \rangle$ single-crystal Al_2O_3 phase and a $\langle 7\,4\,3 \rangle$ single-crystal YAG phase without grain boundaries. The eutectic composite has superior high-temperature strength characteristics with flexural strength showing no temperature dependence in the range from room temperature up to 2073 K. In tensile test at above 1923 K, the composite showed marked plastic deformation occurring by dislocation motion. This eutectic composite has a very thermally stable microstructure with no grain growth in evidence after lengthy heat treatment at a high temperature of 1973 K in an air atmosphere. These excellent high-temperature characteristics are caused by such factors as: first, a single-crystal Al_2O_3 phase/single-crystal YAG phase structure; second, the formation of a compatible interface with no amorphous phase, and stability at high temperature; and finally, the combined effect of a YAG phase with superior high-temperature characteristics.

Acknowledgements

We thank M. Suzuki at Ube Laboratory, Corporate Research & Development, Ube Industries., Ltd, for his assistance in the TEM observations.

References

1. P. LAMICQ, in Proceedings of Japan–Europe Symposium on Composite Materials, Nagoya, June 1–2, 1993, edited by R & D Institute of Metals and Composites for Future Industries in Japan, Japan Industrial Technology Association, Tokyo, (1993) p. 4.
2. T. P. HERBELL, A. J. ECKEL, D. R. HULL and A. K. MISRA, "Environmental effects on advanced materials", edited by R. H. Jones and R. E. Ricker (The Minerals, Metals & Materials Society, Pennsylvania, 1991) p. 159.
3. K. TSUKUMA, K. UEDA and M. SHIMADA, *J. Amer. Ceram. Soc.* **68** (1985) c-4.
4. K. NIIHARA, A. NAKAHIRA, T. UCHIYAMA and T. HIRAI, "Fracture Mechanics of Ceramics" Vol. 7 (Plenum Press, New York, 1986) p. 103.
5. K. NIIHARA, A. NAKAHIRA, G. SASAKI and M. HIRABAYASHI, in Proceedings of MRS International Meeting on Advanced Materials (Materials Research Society, Plenum, Tokyo, 1989) p. 129.
6. R. MATSUKI, H. UEDA, T. TAKENOUCHI, A. NAKAHIRA and K. NIIHARA, *J. Jpn Soc. Powd. Powd. Metall.* **38** (1991) 365.
7. K. NIIHARA, *ibid* **37** (1990) 348.
8. D. VIECHNICKI and F. SCHMID, *J. Mater. Sci.* **4** (1969) 84.
9. T. MAH and T. A. PARTHASARATHY, *Ceram. Engng Sci. Proc.* **11** (1990) 1617.
10. T. A. PARTHASARATHY, T. MAH and L. E. MATSON, *ibid.* **11** (1990) 1628.
11. *Idem., J. Amer. Ceram. Sci.* **76** (1993) 29.
12. Y. WAKU, N. NAKAGAWA, H. OHTSUBO, Y. OHSORA and Y. KOHTOKU, *J. Jpn Inst. Metals* **59** (1995) 71.
13. Y. WAKU, H. OTSUBO, N. NAKAGAWA and Y. KOHTOKU, *J. Mater. Sci.* **31** (1996) 4663.

14. Y. WAKU, N. NAKAGAWA, H. OHTSUBO and Y. KOHTOKU, in Proceedings of the 16th International SAMPE Europe Conference of the Society for the Advancement of Material and Process Engineering, Salzburg, Austria, May 30–June 1 (1995) p. 117.
15. D. R. CLARKE, *J. Amer. Ceram. Soc.* **62** (1979) 236.
16. J. ECHIGOYA, S. HAYASHI, K. SASAKI and H. SUTO, *J. Jpn Inst. Metals* **48** (1984) 430.
17. F. WAKAI, Y. KODAMA, S. SAKAGUCHI, N. MURAYAMA, K. IZEKI and K. NIIHARA *Nature* **344** (1990) 421.

Received 1 May
and accepted 24 September 1997